HHS Public Access

Author manuscript

Basic Res Cardiol. Author manuscript; available in PMC 2022 July 21.

Published in final edited form as:

Basic Res Cardiol. ; 115(6): 60. doi:10.1007/s00395-020-00818-8.

Deletion of obscurin immunoglobulin domains Ig58/59 leads to age-dependent cardiac remodeling and arrhythmia

Alyssa Grogan[1], **Andrew Coleman**[2], **Humberto Joca**[2], **Henk Granzier**[3], **Mark W. Russel**[4], **Christopher W. Ward**[2], **Aikaterini Kontrogianni-Konstantopoulos**[1]

[1]Department of Biochemistry and Molecular Biology, University of Maryland School of Medicine, Baltimore, MD 21201, USA

[2]Department of Orthopedics, University of Maryland School of Medicine, Baltimore, MD 21201, USA

[3]Department of Physiology, University of Arizona College of Medicine, Tucson, AZ 85724, USA

[4]Department of Pediatrics and Communicable Diseases, University of Michigan Medical School, Ann Arbor, MI 48109, USA

Abstract

Obscurin comprises a family of giant modular proteins that play key structural and regulatory roles in striated muscles. Immunoglobulin domains 58/59 (Ig58/59) of obscurin mediate binding to essential modulators of muscle structure and function, including canonical titin, a smaller splice variant of titin, termed novex-3, and phospholamban (PLN). Importantly, missense mutations localized within the obscurin-Ig58/59 region that affect binding to titins and/or PLN have been linked to the development of myopathy in humans. To elucidate the pathophysiological role of this region, we generated a constitutive deletion mouse model, *Obscn-ΔIg58/59*, that expresses obscurin lacking Ig58/59, and determined the consequences of this manipulation on cardiac morphology and function under conditions of acute stress and through the physiological process of aging. Our studies show that young *Obscn-ΔIg58/59* mice are susceptible to acute β-adrenergic stress. Moreover, sedentary *Obscn-ΔIg58/59* mice develop left ventricular hypertrophy that progresses to dilation, contractile impairment, atrial enlargement, and arrhythmia as a function of aging with males being more affected than females. Experiments in ventricular cardiomyocytes revealed altered Ca^{2+} cycling associated with changes in the expression and/or phosphorylation levels of major Ca^{2+} cycling proteins, including PLN, SERCA2, and RyR2. Taken together, our work demonstrates that obscurin-Ig58/59 is an essential regulatory module in the heart and its deletion leads to age- and sex-dependent cardiac remodeling, ventricular dilation, and arrhythmia due to deregulated Ca^{2+} cycling.

✉Aikaterini Kontrogianni-Konstantopoulos, akontrogianni@som.umaryland.edu.

Conflict of interest None declared.

Electronic supplementary material The online version of this article (https://doi.org/10.1007/s00395-020-00818-8) contains supplementary material, which is available to authorized users.

Keywords

Obscurin; Hypertrophy; Dilation; Ca^{2+} cycling; Phospholamban; SERCA; Ryanodine receptor; Sex dimorphism

Introduction

Obscurins, expressed from the single *OBSCN* gene, are a family of giant modular proteins (720–870 kDa) surrounding sarcomeric M-bands and Z-disks where they play key structural and regulatory roles [25, 47]. The two canonical isoforms, obscurin A and B, differ in their COOH-termini where obscurin A contains ankyrin-binding sites and obscurin B carries two active serine/threonine kinase domains belonging to the myosin lightchain kinase subfamily [17, 42]. Their modular nature and unique positioning at the periphery of myofibrils allow obscurins to provide binding sites for diverse proteins localized to different subcellular compartments [25, 47]. Consistently, obscurins have been implicated in several cellular processes ranging from myofibril assembly to the integration of the sarcomeric cytoskeleton with the sarcoplasmic reticulum (SR), cell adhesion, the maintenance of the subsarcolemmal microtubule network, and Ca^{2+} signaling [21, 25, 47]. Their pathophysiological significance has been further substantiated by the identification of > 15 missense, splicing, and frameshift mutations in *OBSCN* that have been linked to the development of hypertrophic cardiomyopathy (HCM), dilated cardiomyopathy (DCM), and left ventricular non-compaction (LVNC) in humans [19].

Among the multiple binding partners of obscurins, titin and novex-3 were the first to be identified with obscurin immunoglobulin domains 58/59 (Ig58/59) supporting binding to both titin Ig9/10 and a unique 198-amino acid-long sequence of novex-3 [4, 49]. Titin (3–4 MDa) forms a continuous filament from Z-disks to M-bands and functions as a molecular scaffold during myofibrillogenesis, a spring that generates passive tension, and a mechanosensor that mediates stretch-initiated signaling pathways [18, 25, 30, 31, 47]. Novex-3 (~ 700 kDa), a titin splice variant, extends from Z-disks to I-bands and likely participates in stress-induced cardiac remodeling [24]. More recently, obscurin Ig58/59 was also shown to moderately bind phospholamban (PLN, ~ 5 kDa) [21], a transmembrane protein of the SR that modulates Ca^{2+} cycling by acting as a negative regulator of the sarcoendoplasmic reticulum Ca^{2+} ATPase (SERCA). Importantly, missense mutations within obscurin Ig58/59 that affect binding to titins and/or PLN have been associated with the development of myopathy in humans, suggesting essential roles for these protein complexes in striated muscle pathophysiology [3, 21, 41].

To elucidate the significance of the obscurin Ig58/59 module, we generated a constitutive deletion mouse model, *Obscn-ΔIg58/59*, that expresses obscurin lacking Ig58/59. Our studies show that young (3- to 4-month-old) homozygous *Obscn-ΔIg58/59* mice, which do not show signs of cardiac dysfunction under sedentary conditions, are susceptible to workload-induced arrhythmia. Moreover, sedentary male *Obscn-ΔIg58/59* mice develop compensatory left ventricular (LV) hypertrophy by 6 months of age that progresses to maladaptive ventricular dilation, contractile impairment, atrial enlargement, and severe

arrhythmia by 12 months. Interestingly, female *Obscn-ΔIg58/59* mice do not undergo cardiac remodeling and dysfunction to the same extent as males, indicating the presence of sex dimorphism in the *Obscn-ΔIg58/59* model. Evaluation of LV cardiomyocytes from male *Obscn-ΔIg58/59* mice revealed abnormal Ca^{2+} transients, reduced contractility, and alterations in the expression and/or phosphorylation levels of PLN, SERCA2, and ryanodine receptor 2 (RyR2). Taken together, our findings demonstrate key regulatory roles for obscurin in the heart, specifically highlighting Ig58/59 as an essential module impacting Ca^{2+} homeostasis.

Materials and methods

Gene targeting and generation of Obscn-ΔIg58/59 constitutive deletion mice

The *Obscn-ΔIg58/59* deletion model was produced in parallel with the *Obscn-R4344Q knock-in* model as described previously (GenOway, Lyon, France) [21]. The gene-targeting construct contained isogenic genomic DNA spanning partial intron 59, in which a loxP-FRT-neomycin-FRT cassette was inserted, to partial intron 65, in which a distal loxP site was inserted, to flox exons 60–61 containing Ig58/59. To remove the neomycin resistance cassette along with exons 60–61, animals containing the recombined *OBSCN* allele were bred with Cre recombinase-expressing mice (GenOway). The genotypes of the animals were confirmed by polymerase chain reaction (PCR) utilizing a primer set complimentary to sequences in intron 59 to amplify the wild-type allele (Sense 5′ATC ATAGAGCAGGACTGGACCGTAGCC3′; Anti-sense 5′GACCGATGACCTCCCAAGTTCATACC3′) and another set complimentary to intron 59 and exon 62 to amplify the deletion allele (Sense 5′TGTCATCATAGAGCAGGACTGGACCG3′; Anti-sense 5′CAGGATAGGGTCACAGAATGGTCACTACG3′). F1 mice were backcrossed seven generations into the C57BL/6J mouse line before experimentation. All experiments were performed with homozygous male and female animals. Euthanasia was performed by inhalation anesthesia of 4.5–5% isoflurane until lack of respiration was noted for a minimum of 60 s followed by a secondary physical method (i.e., cervical dislocation or thoracotomy).

All animal care and procedures were conducted under protocols approved by the Institutional Animal Care and Use Committee at the University of Maryland, School of Medicine (UMSOM), and were in accordance with the NIH guidelines (Guide for the Care and Use of Laboratory Animals).

Transthoracic echocardiography

Transthoracic echocardiography was performed on sedentary animals at 3, 6, 9, and 12 months of age at the Physiological Phenotyping Core of UMSOM as previously described [21]. Briefly, mice shaved in the chest area were initially anesthetized with 3% isoflurane in oxygen in an induction chamber and then maintained under 1.5% isoflurane in oxygen via nose cone on a warming pad through the duration of the recording. Two-dimensional cineloops and guided M-mode frames were taken from the parasternal short axis view and mitral valve Doppler measurements were recorded in the apical four chamber view using a 40-MHz probe connected to the Vevo 2100 System (VisualSonics, Toronto, Canada).

Absolute wall thickness was calculated as AWTd + PWTd, where AWTd is diastolic anterior wall thickness and PWTd is diastolic posterior wall thickness. Relative wall thickness was calculated as (AWTd + PWTd)/EDD, where EDD is end-diastolic diameter. End-diastolic volume (EDV) and end-systolic volume (ESV) were calculated as $1.047 \times EDD^3$ and $1.047 \times ESD^3$, respectively, where ESD represents end-systolic diameter. Ejection Fraction was calculated as (EDV−ESV)/EDV × 100 and Fractional Shortening as (EDD−ESV)/EDD.

Surface electrocardiography

Surface electrocardiography (ECG) was performed on sedentary animals at 6 and 12 months of age as described previously [21]. Briefly, mice were placed on a warming pad in a supine position and maintained under anesthesia with 1.5% isoflurane in oxygen via nose cone. Three-lead ECG probes were inserted subcutaneously in which the positive, negative, and ground electrodes were placed in the left hindlimb, right forelimb, and left forelimb, respectively. The electrodes were linked to a biopotential amplifier (BIOPAC MEC100C) connected to a computer interfaced BIOPAC MP150 system (BIOPAC Systems Inc., Goleta, CA) to measure and record electrical signals. Traces for each animal were recorded continuously for 30 min. Heart rate measurements and R–R intervals were calculated using Acqknowledge software.

Isoproterenol challenge

Young (3- to 4-month-old) mice were anesthetized by intraperitoneal (IP) injection of Avertin (1.25% 2-2-2 tribromoethanol, 2.5% 2-methl-2-butanol) at 0.014 ml/g and baseline heart rate was recorded for 5 min by ECG as described above. Isoproterenol was subsequently injected intraperitoneally at a dose of 0.44 μg/kg and cardiac electrical activity was recorded by ECG for another 30 min. The change in heart rate (Δheart rate) was calculated for each mouse as the difference in heart rate before and after isoproterenol treatment.

Lysate preparation and western blotting

Flash-frozen LV tissue was ground to powder in a glass homogenizer while immersed in liquid nitrogen. The ground tissue was incubated at − 20 °C for 20 min and then solubilized in urea–thiourea lysis buffer (8 mol/L urea, 2 mol/L thiourea, 3% SDS, 0.05 mol/L tris–HCl, 0.03% bromophenol blue, 0.075 mol/L dithiothreitol, pH 6.8) and 50% glycerol supplemented with protease and phosphatase inhibitors (Halt Protease and Phosphatase Inhibitor Cocktail, Thermo Fisher Scientific, Rockford, IL) in a 60 °C water bath. Following centrifugation, lysates were aliquoted and flash frozen in liquid nitrogen. Equal amounts of protein lysates were thawed at 55 °C for 5 min and separated by SDS-polyacrylamide gel electrophoresis, transferred to nitrocellulose membrane, and probed with the desired primary antibodies. Immunoreactive bands were visualized with chemiluminescent reagents (NovaBright, Thermo Fisher Scientific, Bedford, MA) after incubation with alkaline phosphatase-conjugated secondary antibodies (goat anti-mouse IgG A3688, 1:3000, Sigma-Aldrich, St. Louis, MO and goat anti-rabbit IgG AB_2337947, 1:3000, Jackson Immunoresearch, West Grove, PA). The number of different biological samples (i.e., hearts) and experimental replicates is included in the respective figure legends. Densitometry was performed with ImageJ and normalized to either GAPDH or Hsp90

as a loading control. To validate the use of GAPDH and Hsp90 as loading controls, we normalized GAPDH and Hsp90 expression to total protein using the corresponding Ponceau stained blots; of note, no statistically significant differences were observed in the expression of GAPDH or Hsp90 between wild-type and *Obscn-ΔIg58/59* lysates (Fig. S1a–c). Figures contain a representative biological replicate for each protein and loading control. Occasional digital adjustment was uniformly applied to representative immunoblots for ease of visualization.

Primary antibodies

The following primary antibodies were used for western blotting (WB) and immunofluorescence (IF) staining: mouse monoclonal antibodies to PLN (WB: 1:5000, IF: 1:200; ab2865, Abcam, Cambridge, MA), SERCA2 (WB: 1:1000, IF: 1:00; MA3-919, Thermo Fisher Scientific, Rockford, IL), RyR2 (WB: 1:1000, IF: 1:300; MA3-925, Thermo Fisher Scientific), GAPDH (WB: 1:15,000; G8795, Millipore, Temecula, CA), PP2A catalytic subunit (WB: 1:1000; 05–421, Millipore), PP2Ce (WB: 1:500; MAB6914, R&D Systems, Minneapolis, MN), α-actinin (IF: 1:100; A7811, Sigma), myosin (WB: 1:10; MF20, Developmental Studies Hybridoma Bank, Iowa City, Iowa), actin (WB: 1:1000; A2172, Millipore), and troponin I (WB: 1 μg/mL; ab10231, Abcam), rabbit monoclonal antibodies to Hsp90 (WB: 1:1000; 4877, Cell Signaling Technologies, Danvers, MA), and rabbit polyclonal antibodies to titin-Z (IF: 3 μg/mL) [26], novex-3 (WB: 1:1000, a generous gift from Dr. Henk Granzier) [4], PLN-pSer16 (WB: 1:1000; 07–052, Millipore), PLN-pThr17 (WB: 1:2000; A010-13AP, Badrilla, Leeds, UK), sAnk1 (WB: 1 μg/mL) [28], RyR2-pSer2808 (WB: 1:2000; ab59225, Abcam), RyR2-pSer2814 (WB: 1:500; A010-31AP, Badrilla), CaMKIIδ (WB: 1:1000; PA5-22168, Thermo Fisher Scientific), CaMKII-pThr287 (WB: 1:1000; PA5-37833, Thermo Fisher Scientific), PP1α (WB: 1:1000; 2582S, Cell Signaling Technologies), PP2A B56α (WB: 1:1000; PA5-90634, Thermo Fisher Scientific), tropomyosin (WB: 1 μg/mL; ab55915, Abcam), obscurin Ig58/59 (WB: 1 μg/mL) [45], and obscurin Ig67 (WB: 1 μg/mL, IF: 3 μg/mL). Antibodies to obscurin Ig67 were generated via immunizing rabbits with mouse GST–Ig67 fusion protein (amino acids 6994–7099, accession number: NP_954603, produced in pGEX-4T-1 vector) and affinity purified from rabbit antiserum using GST and GST-Ig67 columns.

Electrophoresis and coomassie blue staining for titin

LV lysates prepared as described above were loaded onto 16 × 18 cm gels composed of 1% agarose in 1× running buffer (50 mM tris, 0.384 mol/L glycine, 0.1% SDS) and 30% glycerol. Proteins were separated using the Hoefer SE600 unit system at 4 °C for 3 h. Gels were stained with Coomassie Blue, and the expression levels of giant titins were quantified using ImageJ and normalized to myosin heavy chain (MHC) which was used as loading control. The number of different biological samples (i.e., hearts) and experimental replicates is included in the respective figure legends. Figures contain a representative biological replicate depicting titin and MHC expression levels. Occasional digital adjustment was uniformly applied to representative gels for ease of visualization.

Preparation of paraffin embedded cardiac sections and Masson's trichrome staining

Paraffin sections were produced and stained using Masson's Trichrome Kit (Thermo Fisher Scientific) at the Research Histology, Pathology and Imaging Core at the University of Texas M.D. Anderson Cancer Center. Briefly, hearts were fixed in formalin for 24–48 h and sequentially dehydrated in 70, 80, 95, and 100% ethanol. Following xylene washes, samples were embedded in paraffin wax and sectioned at 4 μm. Sections were deparaffinized, hydrated in deionized water, and then placed in Bouin's fluid at 56 °C for 1 h. Sections were stained with Weigert's iron hematoxylin stain for 10 min, Biebrich scarlet–acid fuchsin solution for 5–10 min, phosphotungstic–phosphomolybdic acid solution for 5 min, aniline blue stain solution for 5–10 min, and rinsed with deionized water between each staining step. Sections were placed in 1% acetic acid solution for 1 min and rinsed once more with deionized water before mounting.

Hydroxyproline assay

Hydroxyproline content was measured in flash-frozen LV samples isolated from sedentary 6- and 12-month-old mice as described previously [21]. Approximately, 15–20 mg of tissue was boiled overnight in 0.2 ml of 6 mol/L HCl at 110 °C. The hydrolyzed tissue was added to isopropanol (1:16) and mixed with chloramine-T solution in acetate citrate buffer (final concentration: 0.448% chloramine-T, 0.178 mol/L sodium acetate, 44.5 uM citric acid, 11.14 uM NaOH, and 9.856% isopropanol) for 5 min. Reactions were diluted 1:4 with isopropanol–Ehrlich solution (1.531 mol/L p-dimethylaminobenzaldehyde, 76.1% ethanol, 0.945 mol/L sulfuric acid, and 23.1% isopropanol) and incubated at 55 °C for 1 h. Absorbance values were measured at 558 nm and fibrotic content was calculated using a standard curve and normalized to initial sample mass. At least three experimental replicates were obtained per heart.

Preparation of frozen cardiac sections, immunostaining and confocal microscopy

Frozen LV sections were prepared as described previously [21]., hearts perfused in 2% paraformaldehyde (PFA) in phosphate-buffered saline (PBS) were embedded in 7.5% gelatin and 15% sucrose in PBS and frozen with 2-methylbutane. Samples were sectioned at a thickness of 12 μm, permeabilized with 0.1% Triton X-100 in PBS and incubated in blocking buffer (1 mg/mL BSA, 1 mM sodium azide in PBS) for 1 h. Sections were incubated with the desired primary antibodies prepared in blocking buffer overnight at 4 °C. Samples were then washed with blocking buffer, incubated with Alexa Fluor 488 goat anti-rabbit or Alexa Fluor 568 goat anti-mouse secondary antibodies (1:200; Thermo Fisher Scientific) for 2–3 h, washed again with blocking buffer, mounted with VECTASHIELD mounting medium (Vector Laboratories, Burlingame, CA), and analyzed under a Nikon Spinning Disc confocal microscope (UMSOM Confocal Microscopy Facility).

Electron microscopy

LV tissues were isolated from 12-month-old animals and fixed in 2% paraformaldehyde, 2.5% glutaraldehyde, and 0.1 mol/L PIPES buffer (pH 7.4), washed with 0.1 mol/L PIPES buffer, and post-fixed with 1% osmium tetroxide/1.5% potassium ferrocyanide in 0.1 mol/L PIPES buffer for 1 h at 4 °C. Samples were treated with 1% tannic acid in $H_2 0$ for 15

min, followed by *en bloc* staining with 1% (w/v) uranyl acetate, and dehydration using 30, 50, 70, 90 and 100% ethanol in series. Following dehydration, samples were infiltrated and embedded in Araldite-Epoxy resin (Araldite, EMbed 812; Electron Microscopy Sciences, PA), according to the manufacturer's recommendations. Ultrathin sections at ~ 70 nm thickness were cut on a Leica UC6 ultramicrotome (Leica Microsystems, Inc., Bannockburn, IL), and examined under a Tecnai T12 transmission electron microscope (Thermo Fisher Scientific, Hillsboro, Oregon) operated at 80 kV. Images were acquired with an AMT bottom mount CCD camera and AMT600 software (Advanced Microscopy Techniques, Woburn, MA). All samples were prepared and imaged at the Electron Microscopy Core Imaging Facility of the University of Maryland School of Dentistry.

Cardiomyocyte isolation

Ventricular cardiomyocytes were isolated from 6- and 12-month-old mice using a modified Langendorff perfusion protocol [44]. Mice were heparinized and then anesthetized using 3% isoflurane. Whole hearts were excised, placed in ice cold cell isolation buffer (CIB) [130 mM NaCl, 5.4 mM KCl, 0.5 mM M $gCl_2{\cdot}6H_2O$, 0.33 mM NaH_2PO_4, 10 mM glucose, 25 mM HEPES, 10 mM taurine] containing 0.2 mM EGTA (CIB-EGTA), and cannulated through the aorta. Hearts were perfused in retrograde fashion with CIB-EGTA for 3 min and then for 4 min in CIB supplemented with enzymes [1 mg/mL collagenase (Worthington), 0.06 mg/mL trypsin (Sigma), and 0.06 mg/mL protease type XIV (Sigma P5147)] at 37 °C. Ventricular tissue was minced and subjected to additional digestion in CIB supplemented with enzymes for 4 min at 37 °C. Myocytes were transferred to normal Tyrode's solution (NT) [130 mM NaCl, 5.4 mM KCl, 0.5 mM $MgCl_2{\cdot}6H_2O$, 0.33 mM NaH_2PO_4, 5 mM glucose, 5 mM HEPES], dispersed by trituration with a Pasteur pipette, and ultimately brought to physiological Ca^{2+} to a final concentration of 1.8 mM $CaCl_2$ in NT. Myocytes included in this study were Ca^{2+} tolerant and responsive to electrical stimulation following isolation. Any cells with round edges or other visible membrane damage were excluded.

Ca^{2+} transients and contractility measurements

Experiments were performed in custom fabricated chambers (4-h Day foundation, Towson MD) mounted on an Olympus Ix70 Microscope with a 40× Water 1.15 NA objective. Sarcomere length was monitored with a high-speed camera system (Aurora) and was calculated with Fast Fourier Transform analysis. Ca^{2+} transients were evaluated simultaneously after loading 2 μM Fluo-4-AM (15 min incubation) followed by de-esterification (10 min). Cells were excited with 475 nm light from a xenon arc lamp and paced at 1 Hz (2 ms, square pulses, 40 V) for 30 s recording with a dual PMT fluorescence system (Ionoptix, Westwood, MA). All contractions were averaged for each cell and data were analyzed using an inhome MATLAB script.

Statistical analysis

Statistical significance between age- and gender-matched wild-type and homozygous *Obscn-ΔIg58/59* groups was determined by two-tailed Student's *t* test; genotypes were compared within, but not between, different time points and genders. Error bars represent average values ± SEM. Sample sizes are noted in the corresponding figure legends.

Results

Generation and characterization of the *Obscn-ΔIg58/59* model

To assess the pathophysiological significance of the obscurin Ig58/59 module, we generated a constitutive deletion mouse model, *Obscn-ΔIg58/59*, that expresses obscurin lacking Ig58/59 (Fig. S2a, b). Homozygous *Obscn-ΔIg58/59* mice are viable and exhibit normal growth rates (Fig. S2c). Hearts isolated from young adult (3-month-old) wild-type and *Obscn-ΔIg58/59* mice were comparable in size and gross morphology (Fig. 1a–a'). Morphometric and echocardiography analyses did not reveal alterations in cardiac morphology or function at this stage in *Obscn-ΔIg58/59* male animals (Fig. 1b–b'; Table S1). However, a moderate increase in absolute LV mass and stroke volume was observed in *Obscn-ΔIg58/59* female animals compared to gender-matched wild type (Table S2), suggesting a mild adaptive response that was not accompanied by major alterations in LV dimensions or function.

Evaluation of protein expression utilizing antibodies to obscurin Ig58/59 confirmed the deletion of Ig58/59 in *Obscn-ΔIg58/59* lysates prepared from 3-month-old male LV, while antibodies against Ig67 demonstrated that total protein levels were unaltered; notably, prolonged exposure of obscurin Ig67 immunoblots revealed an up-regulation of obscurin B levels, while short exposure indicated a moderate, not statistically significant, decrease in obscurin A levels in *Obscn-ΔIg58/59* lysates compared to wild type (Fig. 1c–c'). Of note, obscurin B is minimally expressed in normal mouse heart tissue [1, 22]. In agreement with our findings, earlier studies have reported up-regulation of small and large obscurin-kinase transcripts/proteins in hypertrophic mouse myocardia following aortic constriction [8] and in a mouse model carrying the HCM-linked R4344Q obscurin mutation in response to pressure overload [21]. It is, therefore, possible that up-regulation of obscurin-kinase isoforms could reflect a compensatory response or an early manifestation of cardiac disease in young adult *Obscn-ΔIg58/59* animals.

Young adult *Obscn-ΔIg58/59* mice exposed to acute β-adrenergic stress develop tachycardia and severe arrhythmia

Given the absence of an obvious cardiac pathology in young adult *Obscn-ΔIg58/59* mice, we next evaluated their susceptibility to acute cardiac workload in the form of β-adrenergic stimulation. Baseline heart rate (HR) was not different in young (3- to 4-month-old) wild-type and *Obscn-ΔIg58/59* male (Fig. 1d) or female (Fig. S3a) mice. In contrast, an acute challenge with a low dose of isoproterenol (0.44 μg/kg) significantly increased HR in both male and female *Obscn-ΔIg58/59* mice compared to their gender-matched wild-type counterparts (Fig. 1d–d'; Fig. S3a–a'). Evaluation of cardiac electrical activity by electrocardiography (ECG) post-isoproterenol revealed normal sinus rhythm in 100% of wild-type female (Fig. S3b and c) and the majority (80%) of wild-type male (Fig. 1e and f) mice, with the remaining 20% of wild-type male mice occasionally showing minor variations in sinus rhythm (Fig. 1f; Fig. S4a). In contrast, ~ 57% of male (Fig. 1e'–f) and 10% of female (Fig. S3b' and c) *Obscn-ΔIg58/59* mice deviated from sinus rhythm with prominent and frequent HR fluctuations, while an additional 10% of female *Obscn-ΔIg58/59* mice exhibited episodes of junctional escape (Fig. S3b"–c).

Taken together, young *Obscn-ΔIg58/59* mice show no apparent pathological phenotype under sedentary conditions, yet manifest with workload-induced arrhythmia following relatively mild β-adrenergic stimulation, with a larger proportion of male *Obscn-ΔIg58/59* mice being affected compared to female.

Sedentary male *Obscn-ΔIg58/59* mice undergo ventricular remodeling and dysfunction as a function of aging

We next evaluated cardiac morphology and function in sedentary wild-type and *Obscn-ΔIg58/59* mice in response to aging. Examination of the gross morphology of the heart did not reveal any differences in size or mass at 6 months in either gender (Fig. 2a–a'; Fig. S5a–a' and Table S1–2). However, echocardiography showed the presence of LV hypertrophy in 6-month-old male *Obscn-ΔIg58/59* mice evidenced by significantly decreased systolic LV internal diameter and end-systolic volume, and increased LV posterior and absolute wall thickness compared to gender- and age-matched wild-type mice (Fig. 2b–b'; Table S1). This remodeling was accompanied by increased LV ejection fraction and fractional shortening, demonstrating enhanced cardiac function in male *Obscn-ΔIg58/59* mice at 6 months (Table S1). Interestingly, echocardiographic assessment of female *Obscn-ΔIg58/59* mice showed neither morphological nor functional alterations, but only a moderate increase in absolute LV mass (Table S2), indicating that compensatory LV hypertrophy manifests in the male gender only.

At 9 months of age, male *Obscn-ΔIg58/59* mice no longer showed significant differences in cardiac morphology or function compared to wild type (Table S1), indicating that they were progressing towards cardiac de-compensation. In contrast, female *Obscn-ΔIg58/59* mice exhibited increased atrial, LV, and whole heart mass normalized to body weight (Table S2). Given that these changes were not accompanied by any functional echocardiographic alterations, this is considered a mild cardiac remodeling with age.

At 12 months of age, the hearts of the male *Obscn-ΔIg58/59* mice exhibited a dramatic enlargement of the LV and atria compared to wild type (Fig. 2a"–a'"; Table S1). Echocardiography further demonstrated LV dilation with significantly increased diastolic and systolic LV internal diameter and end-systolic and -diastolic volumes and decreased relative wall thickness compared to gender- and age-matched wild-type mice (Fig. 2b"–b"'; Table S1). Consistent with a dilated cardiac pathology, male *Obscn-ΔIg58/59* mice exhibited reduced LV ejection fraction and fractional shortening compared to controls (Table S1), signifying the progression from a compensatory hypertrophic phenotype at 6 months to cardiac de-compensation, maladaptive remodeling and dysfunction by 12 months. Interestingly, female *Obscn-ΔIg58/59* mice did not show any significant alterations in cardiac morphology or function by morphometry or echocardiography at 12 months (Table S2 and Fig. S5a"–a"'). The early increase in LV mass that failed to progress with age in females reinforces the presence of sex dimorphism in the *Obscn-ΔIg58/59* model.

Given that fibrosis is a common feature of HCM and DCM and a predictor of cardiac conduction issues and arrhythmia [12, 32], we evaluated LV sections using Masson's Trichrome staining. We observed the presence of peripheral and/or interstitial fibrosis in 12-month-old male and female *Obscn-ΔIg58/59* mice, which was not the case in

age-matched controls and 6-month-old animals of either genotype or gender (Fig. 2c–c'"; Fig. S5b–b'"). Further quantification of collagen content by hydroxyproline assay demonstrated significantly increased fibrosis in both male and female *Obscn-ΔIg58/59* LV at 12 months compared to gender-matched wild-type mice (Fig. 2d; Fig. S5c). Although female *Obscn-ΔIg58/59* mice did not undergo ventricular hypertrophy or dilation, the presence of significant fibrosis at 12 months suggests mild ventricular remodeling.

Given the age-dependent morphological changes present in *Obscn-ΔIg58/59* LV, we evaluated the expression of giant obscurins in wild type and *Obscn-ΔIg58/59* LV at 6 and 12 months of age. Similar to 3-month-old animals, male and female *Obscn-ΔIg58/59* mice did not show alterations in the overall expression of obscurins but revealed a consistent up-regulation of obscurin B at both 6 and 12 months (Fig. 2e–e'; Fig. S5d–d'). To test whether the Ig58/59 deletion impacts the distribution of obscurins, we immunostained LV sections prepared from 12-month-old male wild-type and *Obscn-ΔIg58/59* hearts. Obscurins assumed their proper localization primarily at M-bands (arrowhead) and to a lesser extent at Z-disks (arrow) in both genotypes, as indicated by co-staining with the Z-disk protein α-actinin (Fig. 2f–h'). Furthermore, ultrastructural analysis of 12-month-old male LV sections did not reveal any obvious abnormalities in sarcomere organization in *Obscn-ΔIg58/59* mice (Fig. S6a–a'"). Consistent with this, no changes were observed in the expression levels of myosin, actin, tropomyosin, or troponin I in 12-month-old *Obscn-ΔIg58/59* LV (Fig. S6b–b'), suggesting that sarcomeric proteins are not affected by the Ig58/59 deletion.

Sedentary *Obscn-ΔIg5859* mice develop arrhythmia

The presence of cardiac remodeling at 6 and 12 months of age, albeit different phenotypic manifestation and extent, prompted us to investigate global cardiac electrical activity by ECG. While the average HR was comparable between male wild-type and *Obscn-ΔIg58/59* mice at 6 months (Fig. 3a), Poincare plots depicted increased R–R variability in *Obscn-ΔIg58/59* males (Fig. 3b–b'). Waveform analysis showed no repeated episodes of arrhythmia in wild-type animals (Fig. 3c, d). In contrast, ~ 38% and ~ 13% of 6-month-old male *Obscn-ΔIg58/59* mice displayed frequent episodes of junctional escape and/or atrial fibrillation (AF; Fig. 3c and d') and the presence of premature atrial contractions (PACs; Fig. 3c and d"), respectively. At 6 months, female *Obscn-ΔIg58/59* mice exhibited significant bradycardia compared to gender-matched wild type, perhaps in association with the moderately increased LV mass observed at this stage (Fig. S7a). Similar to male mice, increased R–R variability was also evident in 6-month-old female *Obscn-ΔIg58/59* mice (Fig. S7b–b'). While wild-type females did not develop arrhythmia (Fig. S7c, d), ~ 33% of 6-month-old female *Obscn-ΔIg58/59* mice experienced episodes of junctional escape and/or AF and occasionally developed PACs (Fig. S7c and d'), while ~ 11% also experienced episodes of sinus rhythm variation associated with AF (Fig. S7c and d").

At 12 months of age, male *Obscn-ΔIg58/59* mice showed significant bradycardia (Fig. 4a) and increased R–R variability (Fig. 4b–b') compared to controls. In contrast to male wild-type mice, in which 90% showed normal sinus rhythm (Fig. 4c, d) and only 10% developed mild HR fluctuations (Fig. 4c; Fig. S4a'), ~ 50% of male *Obscn-ΔIg58/59* mice experienced frequent episodes of sinus rhythm variation (Fig. 4c and d'). In addition, ~ 83%

of male *Obscn-ΔIg58/59* mice developed junctional escape and/or paroxysmal AF (Fig. 4c and d"). In the most severe cases, 12-month-old male *Obscn-ΔIg58/59* mice experienced extreme sinus rhythm fluctuations coincident with sustained AF (Fig. 4d'"). While the mean HR was not different between female *Obscn-ΔIg58/59* and wild-type mice at this age (Fig. S7a), increased R–R variability was still apparent in *Obscn-ΔIg58/59* mice (Fig. S7b"–b'"). Moreover, while ~ 83% of aged female wild-type mice showed no signs of arrhythmia (Fig. S7c and e) and only ~ 17% exhibited minor fluctuations in HR (Fig. S7c and S4a"), ~ 38% and ~ 13% of female *Obscn-ΔIg58/59* mice experienced sinus rhythm variation (Fig. S7c and e'–e") and junctional escape (Fig. S7c and e"), respectively.

Taken together, our data show a comparable arrhythmia burden in 6-month-old male and female *Obscn-ΔIg58/59* mice. However, the aging of *Obscn-ΔIg58/59* mice to 12 months uncovers prominent sex dimorphism with arrhythmia frequency elevated and severity enhanced in male mice.

Ventricular cardiomyocytes isolated from male *Obscn-ΔIg58/59* mice exhibit altered contractility and Ca^{2+} cycling

Given the prominent arrhythmia, ventricular remodeling, and contractile dysfunction observed in *Obscn-ΔIg58/59* mice in vivo, we next assessed Ca^{2+} cycling and contractility kinetics in isolated ventricular cardiomyocytes. Due to the presence of more severe pathologies in male *Obscn-ΔIg58/59* mice, we focused our in vitro studies on males. Isolated ventricular cardiomyocytes obtained from male *Obscn-ΔIg58/59* hearts were significantly enlarged compared to age-matched controls at 6 and 12 months of age (Fig. 5a–a"), which is consistent with the ventricular remodeling revealed by echocardiography. To investigate Ca^{2+} cycling and contractility in single cardiomyocytes, Ca^{2+} transients and cell shortening kinetics were measured simultaneously after pacing to steady state under unloaded conditions. Ca^{2+} transients and contractility kinetics were unaltered in ventricular cardiomyocytes from 6-month-old *Obscn-ΔIg58/59* hearts compared to controls (Fig. 5b, c–c'", d, and e–e"), suggesting that the observed arrhythmia may originate in atrial or nodal cells. This notion is supported by our findings indicating that 6-month-old male *Obscn-ΔIg58/59* mice primarily experience junctional escape rhythms, AF, or PACs.

In contrast, ventricular cardiomyocytes from 12-month-old male *Obscn-ΔIg58/59* hearts exhibited increased peak sarcomere length (SL), reduced fractional shortening, decreased contraction and prolonged relaxation times compared to age-matched wild-type cells (Fig. 5b'–c'"); of note, baseline SL and the peak velocities of contraction and relaxation remained unaltered at both 6 and 12 months (Fig. S8a–a"). Moreover, assessment of Ca^{2+} transients revealed elevated baseline Ca^{2+} levels, decreased Ca^{2+} release time, and prolonged Ca^{2+} decay in *Obscn-ΔIg58/59* cells at 12 months (Fig. 5d'–e"), while peak Ca^{2+} and amplitude were unaffected (Fig. S8b–b').

Together these findings indicate that deletion of Ig58/59 leads to abnormalities in Ca^{2+} cycling in aged male *Obscn-ΔIg58/59* cells, which likely underlie the arrhythmia and contractile deficits identified in vivo.

The expression and phosphorylation levels of Ca^{2+} cycling proteins are altered in *Obscn-ΔIg58/59* LV

To gain mechanistic insights underlying the cardiac defects present in *Obscn-ΔIg58/59* mice, we next examined the protein expression levels and phosphorylation status of the Ig58/59 binding partners as well as select Ca^{2+} cycling proteins in male wild-type and *Obscn-ΔIg58/59* LV as a function of aging. No significant changes were observed in the expression or subcellular distribution of giant titins or novex-3 in *Obscn-ΔIg58/59* lysates at 3, 6, or 12 months of age (Fig. 6a, b; Fig. S9a–b'), suggesting that disruption of these complexes does not largely impact these proteins.

At 3 months of age, the expression levels of pentameric and monomeric PLN were unaltered (Fig. 6b–b'). Similarly, the absolute and normalized levels of phosphorylated PLN at Ser16 and Thr17 were also unchanged (Fig. 6b–b'). No significant alterations were observed in the expression or phosphorylation profile of additional Ca^{2+} cycling proteins such as SERCA2, small ankyrin 1 (sAnk1), or RyR2 in *Obscn-ΔIg58/59* lysates compared to controls at this stage (Fig. 6b–b'; Fig. S9a), consistent with the lack of any apparent cardiac (mal)adaptations.

By 6 months of age, when male *Obscn-ΔIg58/59* mice undergo compensatory LV hypertrophy, the expression levels of both pentameric and monomeric PLN were significantly increased in *Obscn-ΔIg58/59* LV (Fig. 6b–b'). Although the normalized levels of phosphorylated pentameric and monomeric PLN at Ser16 were unchanged in *Obscn-ΔIg58/59* LV, the normalized levels of phosphorylated monomeric PLN at Thr17 were decreased by ~ 45% (Fig. 6b–b'), suggesting that the excess monomeric PLN present in *Obscn-ΔIg58/59* LV is un-phosphorylated at Thr17. Elevated levels of monomeric PLN in the un-phosphorylated state would perhaps lead to over-inhibition of SERCA2 in *Obscn-ΔIg58/59* LV that could impair Ca^{2+} removal and decrease contractile kinetics. However, this elevation in PLN was accompanied by a 25% increase in SERCA2 expression in *Obscn-ΔIg58/59* lysates (Fig. 6b–b'), which together align with the observed cardiac compensation in male *Obscn-ΔIg58/59* LV. Analysis of additional Ca^{2+} cycling proteins demonstrated that the expression of sAnk1 (Fig. 6b and Fig. S9a) and the total or phosphorylated levels of RyR2 (Fig. 6b–b') were unaffected in 6-month-old *Obscn-ΔIg58/59* LV.

At 12 months of age, when male *Obscn-ΔIg58/59* mice experience LV dilation, contractile dysfunction, and Ca^{2+} transient abnormalities, the increase in total PLN expression was a strong trend in *Obscn-ΔIg58/59* lysates (Fig. 6b–b'). Although the absolute levels of phosphorylated PLN at Ser16 were increased in *Obscn-ΔIg58/59* lysates, normalization to total PLN expression revealed no difference between genotypes (Fig. 6b–b'), suggesting that the excess PLN in *Obscn-ΔIg58/59* LV is fully phosphorylated on Ser16 at 12 months. In contrast, there was a significant decrease in the absolute levels of phosphorylated pentameric and monomeric PLN at Thr17 in *Obscn-ΔIg58/59* lysates, calculated to be ~ 68% and ~ 77% following normalization to total PLN levels (Fig. 6b–b'). Contrary to 6-month-old *Obscn-ΔIg58/59* hearts, SERCA2 expression was unaltered at 12 months (Fig. 6b–b'). Given that un-phosphorylated PLN is an inhibitor of SERCA2 activity, and that the increased SERCA2 expression was no longer observed at 12 months, these findings provide a plausible mechanism for the prolonged Ca^{2+} decay seen in the 12-month *Obscn-ΔIg58/59*

LV cardiomyocytes. Examination of additional Ca^{2+} cycling proteins showed no changes in the expression of sAnk1 (Fig. 6b and Fig. S9a), and the total or phosphorylated levels of RyR2 at Ser2808 (Fig. 6b–b'). However, the levels of phosphorylated RyR2 at Ser2814 were significantly decreased (~ 20%) in *Obscn-ΔIg58/59* lysates compared to wild type (Fig. 6b–b'). Given that RyR2 phosphorylation enhances its open probability and, therefore, Ca^{2+} release [13], the reduced phosphorylation at Ser2814 would predict decreased RyR2 open probability and the observed reduction in Ca^{2+} release time found in the 12-month *Obscn-ΔIg58/59* ventricular cells.

Notably, the distribution of PLN, SERCA2 and RyR2 was indistinguishable between wild-type and *Obscn-ΔIg58/59* hearts (Fig. S9c–e'); therefore, the differences in their expression and/or phosphorylation levels do not appear to result from improper targeting to their normal location at the SR membrane.

We proceeded in assessing the expression and/or phosphorylation levels of several candidate kinases and phosphatases to determine the molecular basis for the reduced phosphorylation of PLN and RyR2 in 12-month-old *Obscn-ΔIg58/59* LV. Importantly, PLN Thr17 and RyR2 Ser2814 are both phosphorylated by Ca^{2+}/calmodulin-dependent protein kinase II (CaMKII) [46, 48]. Examination of CAMKII expression or phosphorylation at Thr287, an autophosphorylation site that serves as a marker of its activity [15, 43], did not reveal any significant alterations (Fig. S10a–a'). Given that the phosphorylation levels of PLN and RyR2 are also regulated by protein phosphatase type 1 (PP1) and protein phosphatase type 2A (PP2A), two major ser/thr phosphatases in the heart, we then evaluated their expression profile [23, 33]. We found no significant alterations in the levels of the catalytic subunit of PP1α, the catalytic subunit of PP2A, or the regulatory subunit of PP2A (B56α) in *Obscn-ΔIg58/59* LV (Fig. S10a–a'). Lastly, we quantified the levels of protein phosphatase type 2Ce (PP2Ce), which specifically de-phosphorylates PLN Thr17 in the heart [2], but its expression was also unaltered (Fig. S10a–a'). Given these findings, it appears that alterations in the expression of these key enzymes are not responsible for the deregulated PLN or RyR2 phosphorylation in *Obscn-ΔIg58/59* LV, suggesting novel and/or more complex regulatory mechanisms.

Discussion

Earlier studies interrogating the role of obscurin in striated muscles found that it is essential for the organization and cytoskeletal alignment of the SR membranes [27, 29, 40], indirectly implicating it in the regulation of Ca^{2+} homeostasis. Recent evidence however has indicated that obscurin may be directly involved in Ca^{2+} cycling, primarily through binding to PLN [21]. Consistent with this, a mouse model carrying the HCM-linked R4344Q mutation localized to obscurin Ig58, *Obscn-R4344Q*, exhibited a "gain-of-function" phenotype in which increased binding between mutant Ig58 and PLN led to increased SERCA activity, which enhanced Ca^{2+} transients and contractility and predisposed to mild arrhythmia [21]. Our present work utilizing the *Obscn-ΔIg58/59* model represents the reciprocal study in which disrupted binding between obscurin Ig58/59 and PLN leads to a "loss-of-function" phenotype characterized by depressed Ca^{2+} cycling and contractility, extensive ventricular remodeling, and severe arrhythmia in the form of sinus rhythm variation and atrial

fibrillation. Evaluation of the *Obscn-R4344Q* and *Obscn-ΔIg58/59* models indicated that the latter develops a more severe cardiac pathology under sedentary conditions, which is sex dependent and progresses with age. Moreover, our biochemical findings revealed novel mechanistic ramifications in the *Obscn-ΔIg58/59* myocardium involving deregulated phosphorylation of major Ca^{2+} cycling proteins that were not observed in the *Obscn-R4344Q* myocardium. Thus, our current work further highlights the role of obscurin in Ca^{2+} cycling in the heart and provides new insights on the pathophysiological importance of the Ig58/59 module.

Although the Ig58/59 deletion is present from birth, young adult (3-month-old) *Obscn-ΔIg58/59* mice did not show prominent cardiac defects under sedentary conditions. Evaluation of protein expression in *Obscn-ΔIg58/59* ventricular lysates did not reveal any alterations in the levels of total obscurin, the binding partners of Ig58/59, or major Ca^{2+} cycling proteins. However, the increase in the levels of obscurin B seen in *Obscn-ΔIg58/59* lysates as early as 3 months provides evidence of subtle molecular changes and signaling alterations that could contribute to disease development and/or stress susceptibility of the *Obscn-ΔIg58/59* mice. Consistent with this notion, young adult *Obscn-ΔIg58/59* mice developed tachycardia and severe arrhythmia following acute treatment with a low dose of isoproterenol, with a larger proportion of males displaying more prominent episodes than females. Given that previous studies reported isoproterenol dosing of 0.25–3 mg/kg IP for acute cardiac stress in mice [10, 16, 50], our findings with a 0.44 μg/kg dosing paradigm (i.e., ~ 3 orders of magnitude lower) emphasize that young *Obscn-ΔIg58/59* mice are highly sensitive to relatively mild forms of pharmacological stress.

In addition to increased susceptibility to pharmacological stress, our studies revealed the presence of cardiac remodeling, contractile dysfunction, abnormal Ca^{2+} cycling and arrhythmia in sedentary *Obscn-ΔIg58/59* mice with severity increasing with aging. Coinciding with this progressive pathology were age-related alterations in the expression and/or phosphorylation levels of SERCA2, PLN, and RyR2. Importantly, these molecular changes are in line with the observed effects on Ca^{2+} transient kinetics at each age and serve as a mechanistic explanation for the progression from compensated to de-compensated cardiomyopathy. Moreover, these molecular alterations align with the progressively enhanced arrhythmic severity through aging, where the observed depression in Ca^{2+} transient kinetics at 12 months correlates with the most severe arrhythmic manifestation.

Analysis of protein expression and phosphorylation levels demonstrated a significant reduction in the phosphorylation of the CaMKII-regulated phosphorylation sites on PLN (Thr17) and RyR2 (Ser2814) in aged male *Obscn-ΔIg58/59* LV. Aligned with our findings are reports linking decreased CAMKII expression/activity and CaMKII-mediated phosphorylation of PLN and/or RyR2 in a heart failure canine model [34] and a myocardial infarction rat model [36]. Conversely, the expression of the PP1 and PP2A phosphatases, which also regulate the phosphorylation levels of PLN and RyR2, is increased in human patients with end-stage heart failure [11, 37]. Consistent with these observations, a recent study evaluating the crosstalk between these enzymes demonstrated that altered kinase/phosphatase balance leads to disrupted ventricular Ca^{2+} cycling [14]. Given our immunoblotting data evaluating the levels of these enzymes, along with PP2Ce that

specifically targets Thr17 on PLN, we were not able to attribute the reduced phosphorylation of PLN or RyR2 to changes in their expression. It is, therefore, possible that these key enzymes are not responsible for the deregulated PLN or RyR2 phosphorylation in *Obscn-ΔIg58/59* LV, or that the underlying mechanisms are more complex than changes in overall protein levels or single phosphorylation events. The existence of multiple CaMKIIδ splice variants undergoing extensive post-translational modifications [5], and the presence of > 200 regulatory subunits associating with PP1 and four families of regulatory subunits, including multiple isoforms and splice variants, associating with PP2A that affect their enzymatic activities and/or targeting, corroborates with the latter [20]. Conversely, given the consistent up-regulation of obscurin B in *Obscn-ΔIg58/59* LV, which occurs prior to and throughout progressive ventricular remodeling, the deregulated phosphorylation of PLN and RyR2 could reflect the disruption of a novel signaling pathway linked to obscurin kinases. In support of this notion, a recent study demonstrated that UNC-89, the nematode obscurin homolog, interacts directly with PP2A targeting it to the M-band [38], while both kinase domains of UNC-89 bind a novel phosphatase, termed small C-terminal domain phosphatase-like 1 (SCPL-1) [39]. Thus, it is possible that enzymes associated with signaling pathways regulated by the obscurin kinases could be driving the pathological mechanisms in *Obscn-ΔIg58/59* myocardia, which represents an intriguing area to pursue in future studies.

In addition to binding PLN, obscurin Ig58/59 also interacts with canonical titin as well as its smaller splice variant, novex-3, at the Z-disk [4, 49]. Titin is well established as a major structural component of the myofibril, acting as molecular scaffold during myofibrillogenesis, regulating passive tension and elasticity, supporting the stabilization of the thick filament, and functioning as mechanosensor [18, 25, 30, 31, 47]. Novex-3 is less well studied, but has been implicated in stress-induced cardiac remodeling [24]. Given that the expression and localization of canonical titin and novex-3 were unchanged in *Obscn-ΔIg58/59* LV, and the ultrastructure of sarcomeres was undisturbed, we conclude that the obscurin/titin complex does not significantly contribute to the observed cardiac pathology.

A consistent finding throughout our studies was the presence of sex dimorphism in the *Obscn-ΔIg58/59* model. In our experiments with young animals exposed to acute pharmacological stress as well as sedentary aging animals, males were consistently more severely affected. Many studies have reported sex differences in rodent models of cardiac disease in which males are more likely than females to develop LV dilation and heart failure [6]. This is reflective of the progression of heart disease in humans since a lower incidence of cardiovascular disease is reported in premenopausal women compared to age-matched men [6, 35]. Accordingly, estrogen is proposed to serve cardioprotective roles in the female heart [6, 35]. Although it is currently unknown what compensatory or cardioprotective mechanisms might be taking place in female *Obscn-ΔIg58/59* hearts, the differences in phenotypic severity between genders recapitulate the sex dimorphism in human cardiac disease and reinforce the idea that biological sex is a strong regulator of cardiac disease progression.

Our findings utilizing the *Obscn-ΔIg58/59* model are especially intriguing given that the deletion of only two Ig domains within a protein containing > 60 Ig domains leads to prominent cardiomyopathy and arrhythmia. This suggests an overall lack of redundancy among the obscurin Ig domains where Ig58/59 assumes a specialized physiological role in Ca^{2+} cycling and its deletion cannot be compensated for by neighboring Ig domains. The severity of the *Obscn-ΔIg58/59* pathology is surprising given the relatively mild phenotype previously observed in *Obscn*$^{-/-}$ mice which completely lack giant obscurin expression [29]. These early studies reported that obscurin knock-out leads to reduced expression of sAnk1 in the heart, but no indication of cardiomyopathy [29]. It was subsequently suggested that homologous proteins sharing functional redundancy with obscurin, such as obscurin-like 1, can compensate for the loss of obscurin in *Obscn*$^{-/-}$ mice [7, 29]. Placing our current results in the context of the *Obscn*$^{-/-}$ model, it is likely that the Ig58/59 deletion acts in a dominant negative fashion. Thus, it is possible that the expression of a truncated obscurin protein in *Obscn-ΔIg58/59* hearts does not trigger the same compensatory mechanisms as the complete lack of the protein in *Obscn*$^{-/-}$ muscles, thereby leading to more severe remodeling and dysfunction in *Obscn-ΔIg58/59* myocardia.

Moreover, contrary to *Obscn*$^{-/-}$ muscles, *Obscn-ΔIg58/59* muscles do not exhibit altered levels or distribution of sAnk1. Given that the direct interaction between the extreme non-modular COOH-terminus of obscurin-A and sAnk1 has been implicated in the assembly, sarcomeric alignment and maintenance of the SR [9, 27–29], the lack of any obvious alterations in the expression profile of sAnk1 along with our biochemical studies suggest regulatory rather than structural deficits of the SR membranes.

Taken together, our work demonstrates that deletion of obscurin Ig58/59 leads to cardiac remodeling and dysfunction in response to acute pharmacological stress and the physiological process of aging that manifests to different extents between males and females, and results in pathological alterations in the expression and phosphorylation of major Ca^{2+} cycling proteins. Given that mutations within Ig58/59 have been linked to the development of different forms of myopathy in humans, our findings provide important insights on the consequences of such mutations and implicate obscurin Ig58/59 as an essential regulatory module for Ca^{2+} cycling in the heart.

Supplementary Material

Refer to Web version on PubMed Central for supplementary material.

Acknowledgements

The authors wish to thank Dr. Maegen Ackermann for propagating the *Obscn-ΔIg58/59* mouse model and Dr. Li-Yen Rebecca Hu for propagating the *Obscn-ΔIg58/59* mouse model and performing pilot studies.

Funding

This work was supported by the National Institutes of Health [Training Program in Muscle Biology, T32 AR007592-17 to A.G. and A.C., R35HL144998 to H.G, and R01AR071618 and R01AR071614 to C.W.W.]; and the American Heart Association [Grant In Aid 16GRNT31290010 to A.K.K. and AHA 19POST34450156 to H.J.].

References

1. Ackermann MA, Shriver M, Perry NA, Hu LY, Kontrogianni-Konstantopoulos A (2014) Obscurins: goliaths and Davids take over non-muscle tissues. PLoS ONE 9:e88162. 10.1371/journal.pone.0088162 [PubMed: 24516603]
2. Akaike T, Du N, Lu G, Minamisawa S, Wang Y, Ruan H (2017) A sarcoplasmic reticulum localized protein phosphatase regulates phospholamban phosphorylation and promotes ischemia reperfusion injury in the heart. JACC Basic Transl Sci 2:160–180. 10.1016/j.jacbts.2016.12.002 [PubMed: 29057374]
3. Arimura T, Matsumoto Y, Okazaki O, Hayashi T, Takahashi M, Inagaki N, Hinohara K, Ashizawa N, Yano K, Kimura A (2007) Structural analysis of obscurin gene in hypertrophic cardiomyopathy. Biochem Biophys Res Commun 362:281–287. 10.1016/j.bbrc.2007.07.183 [PubMed: 17716621]
4. Bang ML, Centner T, Fornoff F, Geach AJ, Gotthardt M, McNabb M, Witt CC, Labeit D, Gregorio CC, Granzier H, Labeit S (2001) The complete gene sequence of titin, expression of an unusual approximately 700-kDa titin isoform, and its interaction with obscurin identify a novel Z-line to I-band linking system. Circ Res 89:1065–1072. 10.1161/hh2301.100981 [PubMed: 11717165]
5. Beckendorf J, van den Hoogenhof MMG, Backs J (2018) Physiological and unappreciated roles of CaMKII in the heart. Basic Res Cardiol 113:29. 10.1007/s00395-018-0688-8 [PubMed: 29905892]
6. Blenck CL, Harvey PA, Reckelhoff JF, Leinwand LA (2016) The importance of biological sex and estrogen in rodent models of cardiovascular health and disease. Circ Res 118:1294–1312. 10.1161/CIRCRESAHA.116.307509 [PubMed: 27081111]
7. Blondelle J, Marrocco V, Clark M, Desmond P, Myers S, Nguyen J, Wright M, Bremner S, Pierantozzi E, Ward S, Esteve E, Sorrentino V, Ghassemian M, Lange S (2019) Murine obscurin and Obsl1 have functionally redundant roles in sarcolemmal integrity, sarcoplasmic reticulum organization, and muscle metabolism. Commun Biol 2:178. 10.1038/s42003-019-0405-7 [PubMed: 31098411]
8. Borisov AB, Raeker MO, Kontrogianni-Konstantopoulos A, Yang K, Kurnit DM, Bloch RJ, Russell MW (2003) Rapid response of cardiac obscurin gene cluster to aortic stenosis: differential activation of Rho-GEF and MLCK and involvement in hypertrophic growth. Biochem Biophys Res Commun 310:910–918. 10.1016/j.bbrc.2003.09.035 [PubMed: 14550291]
9. Busby B, Willis CD, Ackermann MA, Kontrogianni-Konstantopoulos A, Bloch RJ (2010) Characterization and comparison of two binding sites on obscurin for small ankyrin 1. Biochemistry 49:9948–9956. 10.1021/bi101165p [PubMed: 20949908]
10. Cerrone M, Montnach J, Lin X, Zhao YT, Zhang M, Agullo-Pascual E, Leo-Macias A, Alvarado FJ, Dolgalev I, Karathanos TV, Malkani K, Van Opbergen CJM, van Bavel JJA, Yang HQ, Vasquez C, Tester D, Fowler S, Liang F, Rothenberg E, Heguy A, Morley GE, Coetzee WA, Trayanova NA, Ackerman MJ, van Veen TAB, Valdivia HH, Delmar M (2017) Plakophilin-2 is required for transcription of genes that control calcium cycling and cardiac rhythm. Nat Commun 8:106. 10.1038/s41467-017-00127-0 [PubMed: 28740174]
11. DeGrande ST, Little SC, Nixon DJ, Wright P, Snyder J, Dun W, Murphy N, Kilic A, Higgins R, Binkley PF, Boyden PA, Carnes CA, Anderson ME, Hund TJ, Mohler PJ (2013) Molecular mechanisms underlying cardiac protein phosphatase 2A regulation in heart. J Biol Chem 288:1032–1046. 10.1074/jbc.M112.426957 [PubMed: 23204520]
12. Disertori M, Mase M, Ravelli F (2017) Myocardial fibrosis predicts ventricular tachyarrhythmias. Trends Cardiovasc Med 27:363–372. 10.1016/j.tcm.2017.01.011 [PubMed: 28262437]
13. Dobrev D, Wehrens XH (2014) Role of RyR2 phosphorylation in heart failure and arrhythmias: controversies around ryanodine receptor phosphorylation in cardiac disease. Circ Res 114:1311–1319. 10.1161/circresaha.114.300568 (discussion 1319) [PubMed: 24723656]
14. Eiringhaus J, Herting J, Schatter F, Nikolaev VO, Sprenger J, Wang Y, Kohn M, Zabel M, El-Armouche A, Hasenfuss G, Sossalla S, Fischer TH (2019) Protein kinase/phosphatase balance mediates the effects of increased late sodium current on ventricular calcium cycling. Basic Res Cardiol 114:13. 10.1007/s00395-019-0720-7 [PubMed: 30788598]
15. Erickson JR (2014) Mechanisms of CaMKII Activation in the Heart. Front Pharmacol 5:59. 10.3389/fphar.2014.00059 [PubMed: 24765077]

16. Feng Y, Cheng J, Wei B, Wang Y (2017) CaMKII inhibition reduces isoproterenol-induced ischemia and arrhythmias in hypertrophic mice. Oncotarget 8:17504–17509. 10.18632/oncotarget.15099 [PubMed: 28177919]
17. Fukuzawa A, Idowu S, Gautel M (2005) Complete human gene structure of obscurin: implications for isoform generation by differential splicing. J Muscle Res Cell Motil 26:427–434. 10.1007/s10974-005-9025-6 [PubMed: 16625316]
18. Gautel M (2011) Cytoskeletal protein kinases: titin and its relations in mechanosensing. Pflugers Arch 462:119–134. 10.1007/s00424-011-0946-1 [PubMed: 21416260]
19. Grogan A, Kontrogianni-Konstantopoulos A (2019) Unraveling obscurins in heart disease. Pflugers Arch 471:735–743. 10.1007/s00424-018-2191-3 [PubMed: 30099631]
20. Heijman J, Dewenter M, El-Armouche A, Dobrev D (2013) Function and regulation of serine/threonine phosphatases in the healthy and diseased heart. J Mol Cell Cardiol 64:90–98. 10.1016/j.yjmcc.2013.09.006 [PubMed: 24051368]
21. Hu LR, Ackermann MA, Hecker PA, Prosser BL, King B, O'Connell KA, Grogan A, Meyer LC, Berndsen CE, Wright NT, Jonathan Lederer W, Kontrogianni-Konstantopoulos A (2017) Deregulated Ca(2+) cycling underlies the development of arrhythmia and heart disease due to mutant obscurin. Sci Adv 3:e1603081. 10.1126/sciadv.1603081 [PubMed: 28630914]
22. Hu LY, Kontrogianni-Konstantopoulos A (2013) The kinase domains of obscurin interact with intercellular adhesion proteins. FASEB J 27:2001–2012. 10.1096/fj.12-221317 [PubMed: 23392350]
23. Huke S, Bers DM (2008) Ryanodine receptor phosphorylation at Serine 2030, 2808 and 2814 in rat cardiomyocytes. Biochem Biophys Res Commun 376:80–85. 10.1016/j.bbrc.2008.08.084 [PubMed: 18755143]
24. Kellermayer D, Smith JE 3rd, Granzier H (2017) Novex-3, the tiny titin of muscle. Biophys Rev 9:201–206. 10.1007/s12551-017-0261-y [PubMed: 28510117]
25. Kontrogianni-Konstantopoulos A, Ackermann MA, Bowman AL, Yap SV, Bloch RJ (2009) Muscle giants: molecular scaffolds in sarcomerogenesis. Physiol Rev 89:1217–1267. 10.1152/physrev.00017.2009 [PubMed: 19789381]
26. Kontrogianni-Konstantopoulos A, Catino DH, Strong JC, Bloch RJ (2006) De novo myofibrillogenesis in C2C12 cells: evidence for the independent assembly of M bands and Z disks. Am J Physiol Cell Physiol 290:C626–C637. 10.1152/ajpcell.00442.2005 [PubMed: 16207790]
27. Kontrogianni-Konstantopoulos A, Catino DH, Strong JC, Sutter S, Borisov AB, Pumplin DW, Russell MW, Bloch RJ (2006) Obscurin modulates the assembly and organization of sarcomeres and the sarcoplasmic reticulum. FASEB J 20:2102–2111. 10.1096/fj.06-5761com [PubMed: 17012262]
28. Kontrogianni-Konstantopoulos A, Jones EM, Van Rossum DB, Bloch RJ (2003) Obscurin is a ligand for small ankyrin 1 in skeletal muscle. Mol Biol Cell 14:1138–1148. 10.1091/mbc.e02-07-0411 [PubMed: 12631729]
29. Lange S, Ouyang K, Meyer G, Cui L, Cheng H, Lieber RL, Chen J (2009) Obscurin determines the architecture of the longitudinal sarcoplasmic reticulum. J Cell Sci 122:2640–2650. 10.1242/jcs.046193 [PubMed: 19584095]
30. Linke WA (2018) Titin Gene and protein functions in passive and active muscle. Annu Rev Physiol 80:389–411. 10.1146/annurev-physiol-021317-121234 [PubMed: 29131758]
31. Linke WA, Hamdani N (2014) Gigantic business: titin properties and function through thick and thin. Circ Res 114:1052–1068. 10.1161/CIRCRESAHA.114.301286 [PubMed: 24625729]
32. Louzao-Martinez L, Vink A, Harakalova M, Asselbergs FW, Verhaar MC, Cheng C (2016) Characteristic adaptations of the extracellular matrix in dilated cardiomyopathy. Int J Cardiol 220:634–646. 10.1016/j.ijcard.2016.06.253 [PubMed: 27391006]
33. MacDougall LK, Jones LR, Cohen P (1991) Identification of the major protein phosphatases in mammalian cardiac muscle which dephosphorylate phospholamban. Eur J Biochem 196:725–734. 10.1111/j.1432-1033.1991.tb15871.x [PubMed: 1849481]
34. Mishra S, Sabbah HN, Jain JC, Gupta RC (2003) Reduced Ca^{2+}-calmodulin-dependent protein kinase activity and expression in LV myocardium of dogs with heart failure. Am J Physiol Heart Circ Physiol 284:H876–H883. 10.1152/ajpheart.00266.2002 [PubMed: 12424092]

35. Murphy E, Steenbergen C (2014) Estrogen regulation of protein expression and signaling pathways in the heart. Biol Sex Differ 5:6. 10.1186/2042-6410-5-6 [PubMed: 24612699]
36. Netticadan T, Temsah RM, Kawabata K, Dhalla NS (2000) Sarcoplasmic reticulum Ca(2+)/Calmodulin-dependent protein kinase is altered in heart failure. Circ Res 86:596–605. 10.1161/01.res.86.5.596 [PubMed: 10720422]
37. Neumann J, Eschenhagen T, Jones LR, Linck B, Schmitz W, Scholz H, Zimmermann N (1997) Increased expression of cardiac phosphatases in patients with end-stage heart failure. J Mol Cell Cardiol 29:265–272. 10.1006/jmcc.1996.0271 [PubMed: 9040041]
38. Qadota H, Matsunaga Y, Bagchi P, Lange KI, Carrier KJ, Pols WV, Swartzbaugh E, Wilson KJ, Srayko M, Pallas DC, Benian GM (2018) Protein phosphatase 2A is crucial for sarcomere organization in *Caenorhabditis elegans* striated muscle. Mol Biol Cell 29:2084–2097. 10.1091/mbc.E18-03-0192 [PubMed: 29949401]
39. Qadota H, McGaha LA, Mercer KB, Stark TJ, Ferrara TM, Benian GM (2008) A novel protein phosphatase is a binding partner for the protein kinase domains of UNC-89 (Obscurin) in Caenorhabditis elegans. Mol Biol Cell 19:2424–2432. 10.1091/mbc.E08-01-0053 [PubMed: 18337465]
40. Raeker MO, Su F, Geisler SB, Borisov AB, Kontrogianni-Konstantopoulos A, Lyons SE, Russell MW (2006) Obscurin is required for the lateral alignment of striated myofibrils in zebrafish. Dev Dyn 235:2018–2029. 10.1002/dvdy.20812 [PubMed: 16779859]
41. Rossi D, Palmio J, Evila A, Galli L, Barone V, Caldwell TA, Policke RA, Aldkheil E, Berndsen CE, Wright NT, Malfatti E, Brochier G, Pierantozzi E, Jordanova A, Guergueltcheva V, Romero NB, Hackman P, Eymard B, Udd B, Sorrentino V (2017) A novel FLNC frameshift and an OBSCN variant in a family with distal muscular dystrophy. PLoS ONE 12:e0186642. 10.1371/journal.pone.0186642 [PubMed: 29073160]
42. Russell MW, Raeker MO, Korytkowski KA, Sonneman KJ (2002) Identification, tissue expression and chromosomal localization of human Obscurin-MLCK, a member of the titin and Dbl families of myosin light chain kinases. Gene 282:237–246. 10.1016/s0378-1119(01)00795-8 [PubMed: 11814696]
43. Schulman H, Anderson ME (2010) Ca/calmodulin-dependent protein kinase II in heart failure. Drug Discov Today Dis Mech 7:e117–e122. 10.1016/j.ddmec.2010.07.005 [PubMed: 21503275]
44. Shioya T (2007) A simple technique for isolating healthy heart cells from mouse models. J Physiol Sci 57:327–335. 10.2170/physiolsci.RP010107 [PubMed: 17980092]
45. Shriver M, Stroka KM, Vitolo MI, Martin S, Huso DL, Konstantopoulos K, Kontrogianni-Konstantopoulos A (2015) Loss of giant obscurins from breast epithelium promotes epithelial-to-mesenchymal transition, tumorigenicity and metastasis. Oncogene 34:4248–4259. 10.1038/onc.2014.358 [PubMed: 25381817]
46. Simmerman HK, Collins JH, Theibert JL, Wegener AD, Jones LR (1986) Sequence analysis of phospholamban. Identification of phosphorylation sites and two major structural domains. J Biol Chem 261:13333–13341 [PubMed: 3759968]
47. Wang L, Geist J, Grogan A, Hu LR, Kontrogianni-Konstantopoulos A (2018) Thick filament protein network, functions, and disease association. Compr Physiol 8:631–709. 10.1002/cphy.c170023 [PubMed: 29687901]
48. Wehrens XH, Lehnart SE, Reiken SR, Marks AR (2004) Ca2 +/calmodulin-dependent protein kinase II phosphorylation regulates the cardiac ryanodine receptor. Circ Res 94:e61–e70. 10.1161/01.RES.0000125626.33738.E2 [PubMed: 15016728]
49. Young P, Ehler E, Gautel M (2001) Obscurin, a giant sarcomeric Rho guanine nucleotide exchange factor protein involved in sarcomere assembly. J Cell Biol 154:123–136. 10.1083/jcb.200102110 [PubMed: 11448995]
50. Yuan Q, Fan GC, Dong M, Altschafl B, Diwan A, Ren X, Hahn HH, Zhao W, Waggoner JR, Jones LR, Jones WK, Bers DM, Dorn GW 2nd, Wang HS, Valdivia HH, Chu G, Kranias EG (2007) Sarcoplasmic reticulum calcium overloading in junction deficiency enhances cardiac contractility but increases ventricular automaticity. Circulation 115:300–309. 10.1161/CIRCULATIONAHA.106.654699 [PubMed: 17224479]

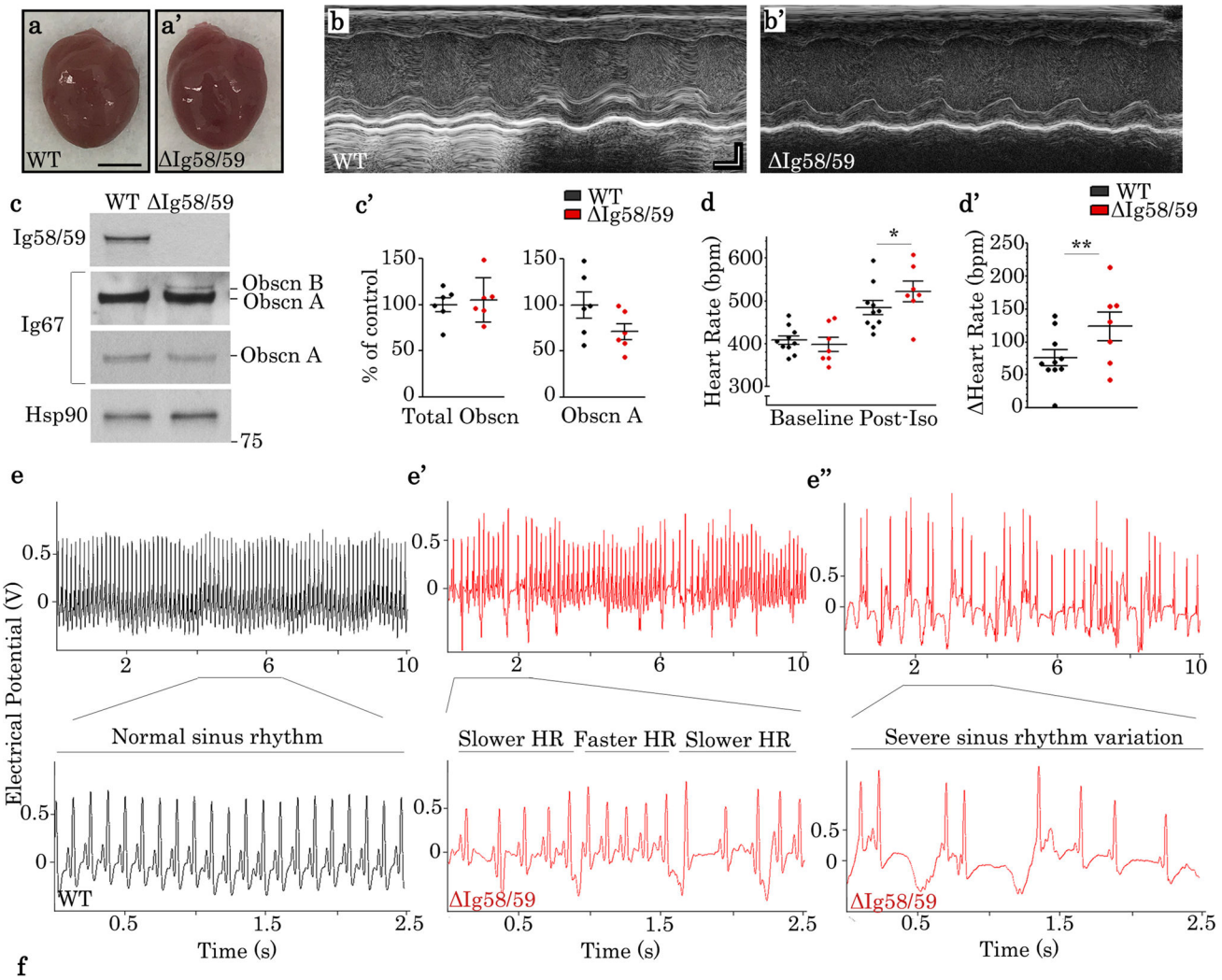

f

	WT (n=10)	ΔIg58/59 (n=7)
Total # of male mice with sinus rhythm variation	2 (20%)	4 (57.1%)

Fig. 1.

Young male *Obscn-ΔIg5859* mice exposed to acute β-adrenergic stress develop tachycardia and severe arrhythmia. **a–a'** Sedentary 3-month-old male wild-type (**a**) and *Obscn-ΔIg5859* (**a'**) hearts demonstrated comparable gross morphologies; scale bar: 3 mm. **b–b'** Echocardiograms obtained from sedentary 3-month-old male wild-type (**b**) and *Obscn-ΔIg5859* (**b'**) mice did not show changes in LV morphology or function; scale bar: 1 mm (vertical axis), 50 ms (horizontal axis). **c–c'** Immunoblotting (**c**) and relative expression (**c'**) of giant obscurins in lysates prepared from sedentary 3-month-old male wild-type and *Obscn-ΔIg5859* LV. Antibodies to obscurin Ig58/59 confirmed the deletion, whereas antibodies to obscurin Ig67 showed that total obscurin levels are unaltered; *t* test, $p = 0.69$. Prolonged exposure of Ig67 immunoblots (top blot) revealed an increase in the levels of obscurin B in *Obscn-ΔIg5859* lysates, which was associated with a moderate, but not significant, decrease in obscurin A levels (bottom blot); *t* test, $p = 0.12$; n = 3 animals

per group; data points represent technical replicas of three different biological samples; Hsp90 served as loading control. **d–d'** Young adult (3–4-month-old) male wild-type and *Obscn-ΔIg5859* mice did not show differences in baseline HR, but *Obscn-ΔIg5859* mice developed significantly elevated HR compared to wild type following acute isoproterenol treatment (**d**). Calculation of ΔHR demonstrated that *Obscn-ΔIg5859* mice experienced a larger increase in HR in response to acute isoproterenol stress (**d'**); *t* test, $*p < 0.05$, $**p < 0.01$; $n = 10$ (wild type), $n = 7$ (*Obscn-ΔIg5859*); data points represent individual animals. **e–e"** Representative ECG traces showed normal sinus rhythm in wild-type mice (**e**) whereas *Obscn-ΔIg5859* animals displayed severe sinus rhythm variation following acute isoproterenol stress (**e'**–**e"**). **f** The number and percentage of animals in each group that experienced arrhythmia following acute isoproterenol treatment is shown; of note, one wild-type animal also experienced minor junctional escape rhythm in response to isoproterenol. WT, wild type; ΔIg5859, *Obscn-ΔIg5859*; Obscn, obscurin; Iso, isoproterenol

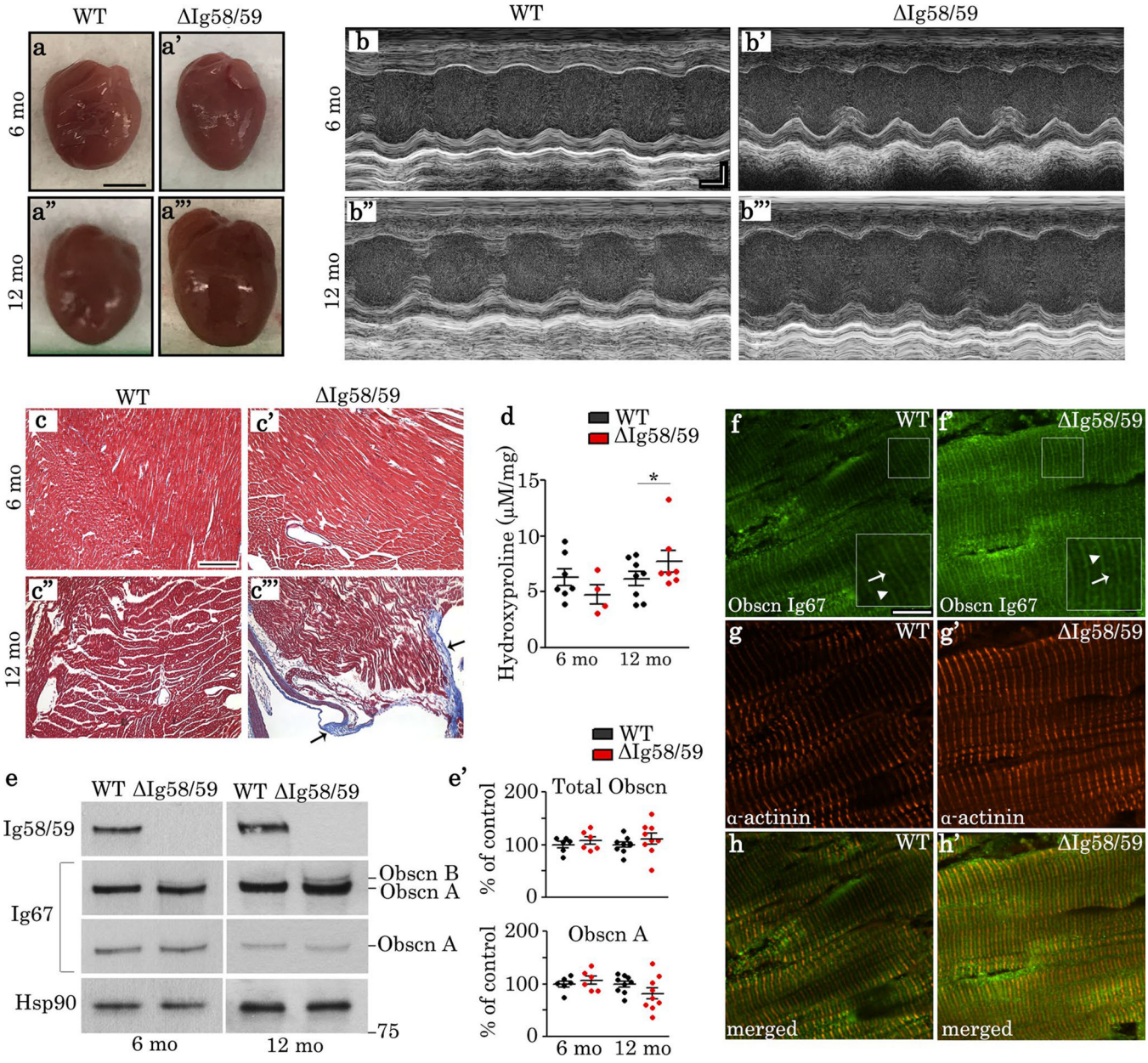

Fig. 2.

Male *Obscn-ΔIg5859* mice develop compensatory LV hypertrophy at 6 months of age that progresses to maladaptive dilation at 12 months. **a–a'"** Gross morphology of sedentary 6- and 12-month-old male wild-type and *Obscn-ΔIg5859* hearts demonstrated atrial enlargement and increased heart size in 12-month-old *Obscn-ΔIg5859* mice (**a'"**) compared to age-matched controls (**a"**), whereas 6-month-old wild-type and *Obscn-ΔIg5859* hearts were comparable in size (**a–a'**); scale bar: 3 mm. **b–b'"** Echocardiograms obtained from sedentary 6- and 12-month-old male wild-type and *Obscn-ΔIg5859* animals demonstrated LV hypertrophy in 6-month-old *Obscn-ΔIg5859* animals (**b'**) and LV dilation in 12-month-old *Obscn-ΔIg5859* mice (**b'"**) compared to age-matched controls (**b** and **b"**); scale bar: 1 mm (vertical axis), 50 ms (horizontal axis). **c–c'"** Masson's Trichrome staining revealed

the presence of peripheral fibrosis (black arrows) in 12-month-old male *Obscn-ΔIg5859* LV (**c'"**); scale bar: 200 μm. **d** Quantitative assessment of fibrosis demonstrated increased hydroxyproline content in male *Obscn-ΔIg5859* LV compared to wild type at 12 months; *t* test: **p* < 0.05; *n* = 7 (6-month-old wild type), *n* = 4 (6-month-old *Obscn-ΔIg5859*), *n* = 8 (12-month-old wild type), *n* = 7 (12-month-old *Obscn-ΔIg5859*); data points represent biological replicates. **e–e'** Immunoblotting (**e**) and relative expression (**e'**) of giant obscurins in lysates prepared from 6- and 12-month-old wild-type and *Obscn-ΔIg5859* LV. Antibodies to obscurin Ig58/59 confirmed the deletion, whereas antibodies to obscurin Ig67 showed that total obscurin expression is unaltered; *t* test, *p* = 0.42 (6 months), *p* = 0.33 (12 months). Prolonged exposures of Ig67 immunoblots (top blot) revealed an increase in the obscurin B levels in *Obscn-ΔIg5859* lysates, which was associated with a moderate, but not significant, decrease in obscurin A levels (bottom blot); *t* test, *p* = 0.50 (6 months), *p* = 0.16 (12 months); *n* = 3 animals per group; data points represent technical replicas of three different biological samples; Hsp90 served as loading control. **f–h'** Immunostained LV sections from 12-month-old male wild-type and *Obscn-ΔIg5859* mice labeled with antibodies to obscurin Ig67 (**f–f'**) and α-actinin as a Z-disk marker (**g–g'**) demonstrated proper localization of obscurins to both M-bands (arrowhead) and Z-disks (arrow); scale bar: 10 μm

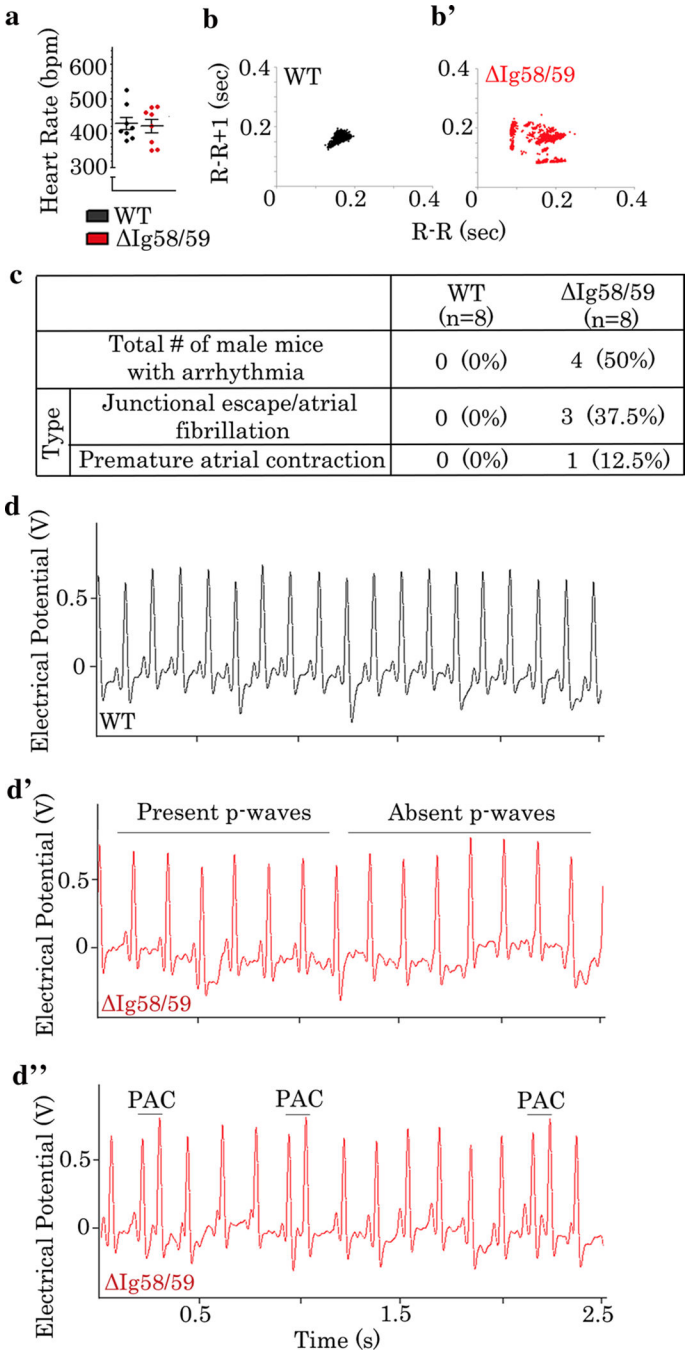

		WT (n=8)	ΔIg58/59 (n=8)
Total # of male mice with arrhythmia		0 (0%)	4 (50%)
Type	Junctional escape/atrial fibrillation	0 (0%)	3 (37.5%)
	Premature atrial contraction	0 (0%)	1 (12.5%)

Fig. 3.

Sedentary male *Obscn-ΔIg5859* mice exhibit atrial arrhythmia at 6 months of age. **a** Sedentary 6-month-old male wild-type and *Obscn-ΔIg5859* mice did not show differences in HR; *t* test, $p = 0.61$; $n = 8$ (wild type), $n = 8$ (*Obscn-ΔIg5859*); data points represent individual animals. **b**–**b'** Poincaré plots demonstrated increased R–R interval variability in *Obscn-ΔIg5859* mice (**b'**) compared to wild type (**b**) at 6 months. **c** The number and percentage of sedentary 6-month-old male wild-type and *Obscn-ΔIg5859* animals that experienced each type of arrhythmia is shown; of note, one wild-type male experienced

a single episode of junctional escape and sinus rhythm variation which was not considered to be severe. **d–d”** Representative ECG traces of sedentary 6-month-old male wild-type (**d**) and *Obscn-ΔIg5859* (**d’–d”**) mice indicated the presence of junctional escape rhythm (**d’**) and repeated PACs (**d”**) in the *Obscn-ΔIg5859* model

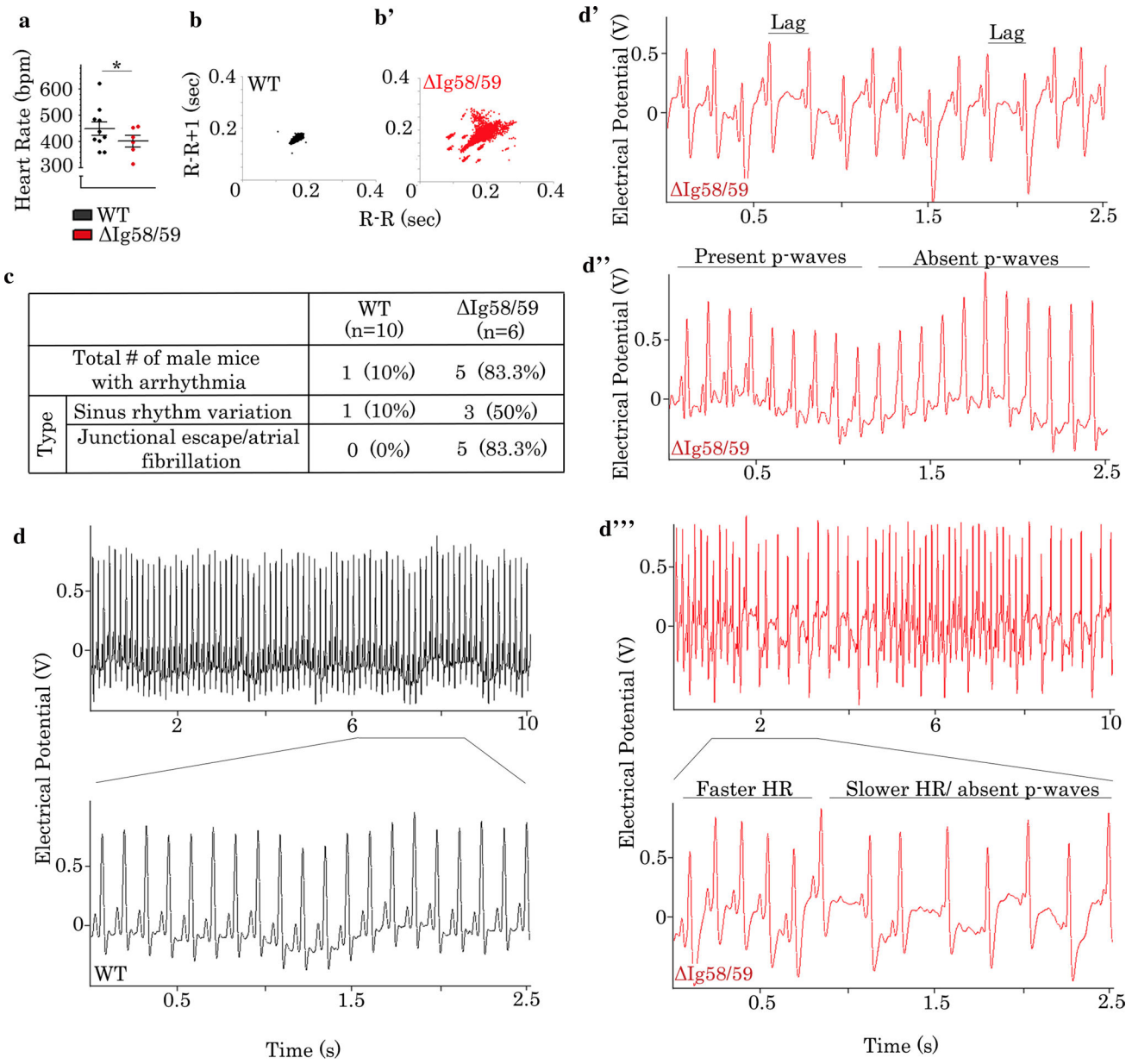

c

		WT (n=10)	ΔIg58/59 (n=6)
Total # of male mice with arrhythmia		1 (10%)	5 (83.3%)
Type	Sinus rhythm variation	1 (10%)	3 (50%)
	Junctional escape/atrial fibrillation	0 (0%)	5 (83.3%)

Fig. 4.

Sedentary male *Obscn-ΔIg5859* mice develop bradycardia and severe arrhythmia at 12 months of age. **a** Sedentary 12-month-old male *Obscn-ΔIg5859* mice demonstrated significant bradycardia compared to wild type; *t* test, $*p < 0.05$; $n = 10$ (wild type), $n = 6$ (*Obscn-ΔIg5859*); data points represent individual animals. **b–b'** Poincaré plots demonstrated increased R–R interval variability in *Obscn-ΔIg5859* mice (**b'**) compared to wild type (**b**) at 12 months. **c** The number and percentage of 12-month-old male wild-type and *Obscn-ΔIg5859* animals that experienced each type of arrhythmia under sedentary conditions is shown. **d–d''** Representative ECG traces of sedentary 12-month-old male wild-type (**d**) and *Obscn-ΔIg5859* (**d'–d'''**) mice revealed the presence of sinus rhythm

variation (**d’**) and junctional escape (**d”**) in the *Obscn-ΔIg5859* model, with more severe cases presenting both arrhythmic phenotypes simultaneously (**d’”**)

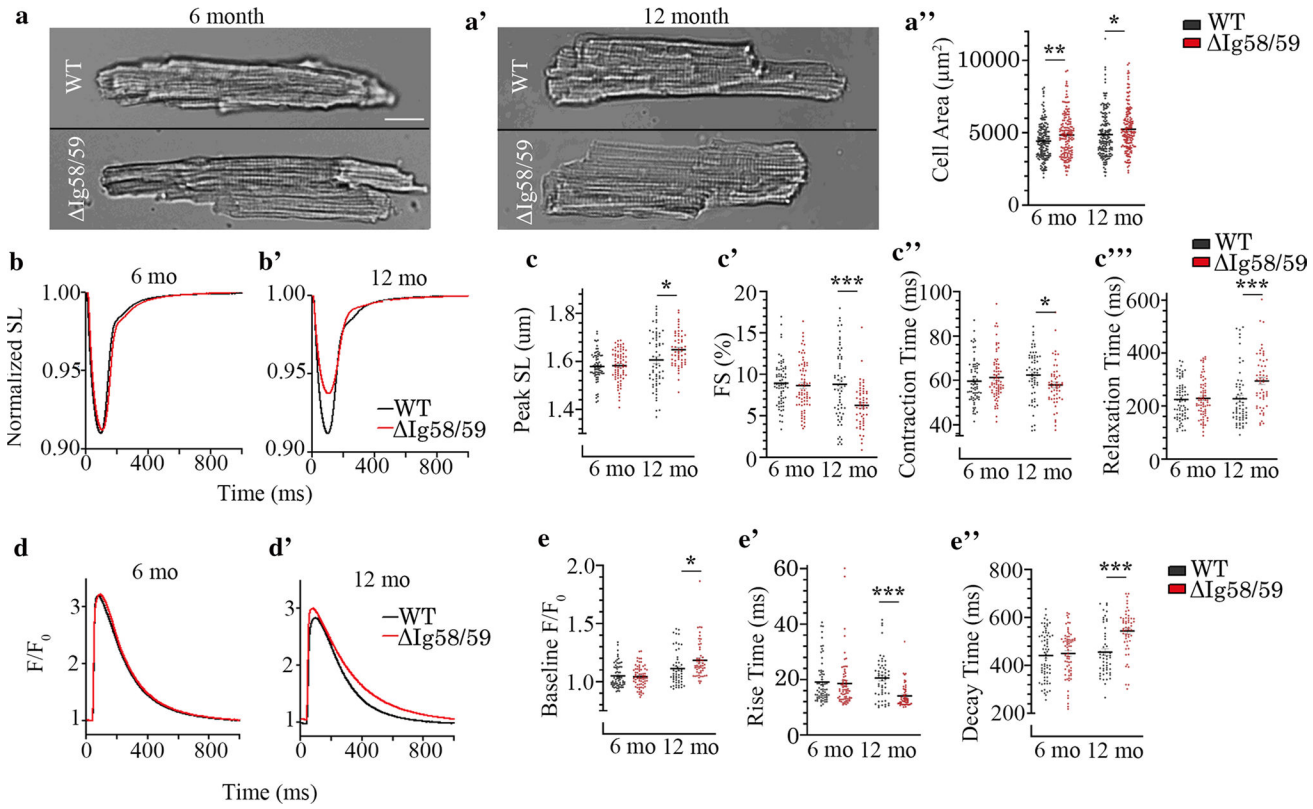

Fig. 5.

Ventricular cardiomyocytes isolated from *Obscn-ΔIg5859* hearts exhibit altered Ca^{2+} cycling and contractility kinetics. **a–a”** Isolated cardiomyocytes from *Obscn-ΔIg5859* ventricles were enlarged at 6 and 12 months of age compared to age-matched wild type; scale bar: 20 μm; *t* test, $*p < 0.05$, $**p < 0.01$; $n = 2$ animals per group, 150–160 cells per group; data points represent individual cells. **b–c’”** Ventricular cardiomyocytes obtained from 6-month-old male wild-type and *Obscn-ΔIg5859* mice did not show differences in contractility (**b** and **c–c’”**), whereas 12-month-old male *Obscn-ΔIg5859* cells showed increased peak SL, reduced fractional shortening (FS), and altered contractility kinetics (**b’** and **c–c’”**) compared to age-matched wild type. **d–e”** Ventricular cardiomyocytes isolated from 6-month-old male wild-type and *Obscn-ΔIg5859* mice did not show differences in Ca^{2+} transients (**d** and **e–e”**), whereas 12-month-old male *Obscn-ΔIg5859* mice exhibited elevated baseline Ca^{2+}, reduced Ca^{2+} release time, and prolonged Ca^{2+} decay time (**d’** and **e–e”**) compared to age-matched wild type; *t* test, $*p < 0.05$, $***p < 0.001$; $n = 4$ animals per group, 50–70 cells per group; data points represent individual cells

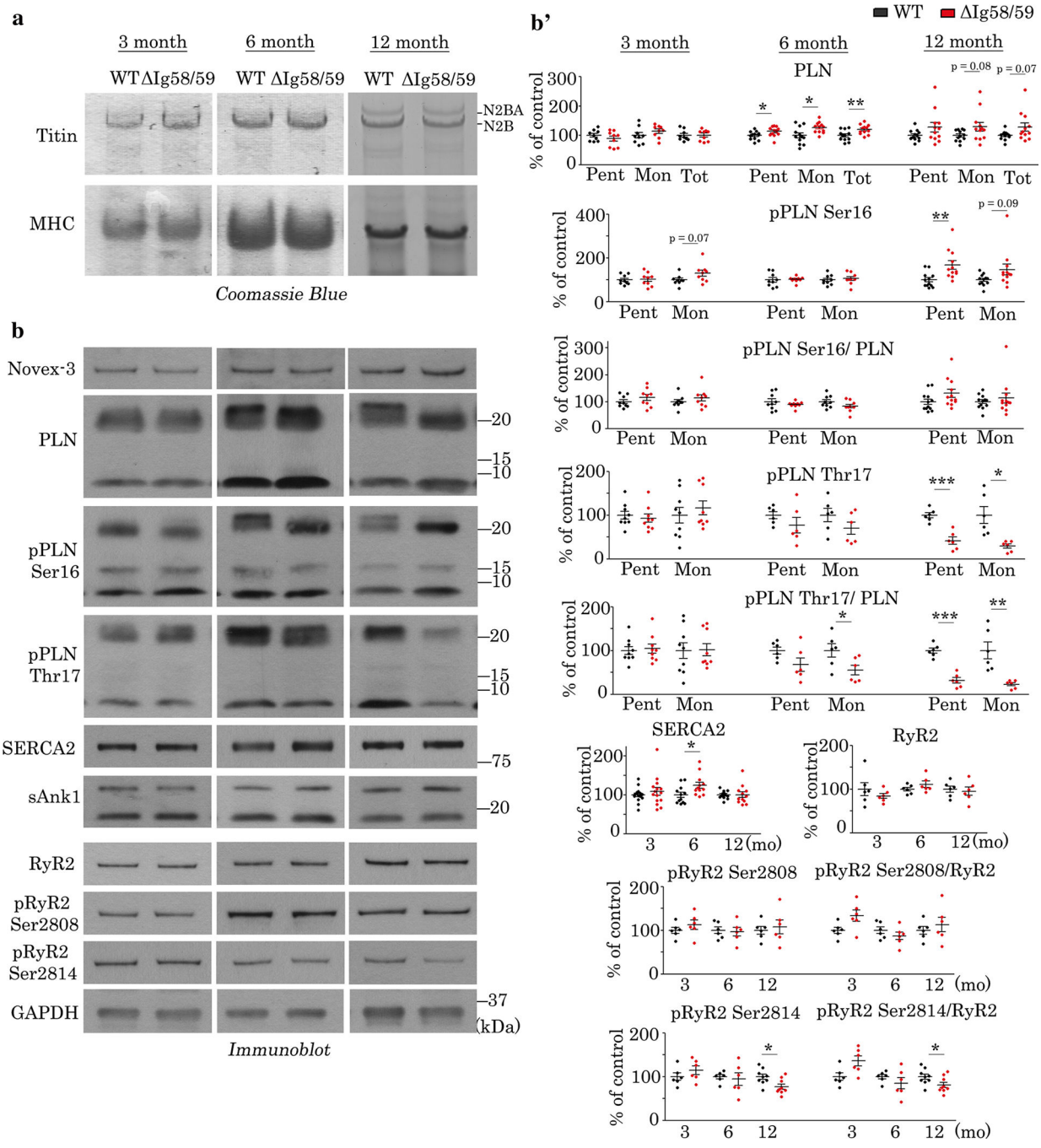

Fig. 6.

Altered expression and phosphorylation levels of Ca^{2+} cycling proteins in *Obscn-ΔIg5859* LV. **a** Coomassie stained agarose gels did not show alterations in the expression of titins in lysates prepared from 3-, 6- and 12-month-old male LV; $n = 3$ animals per group; myosin heavy chain (MHC) served as loading control. **b–b'** Immunoblotting (**b**) and relative expression (**b'**) of lysates prepared from 3-, 6- and 12-month-old male LV with antibodies against the binding partners of Ig58/59 and select Ca^{2+} cycling proteins revealed age-dependent alterations in the expression of PLN and its phosphorylation at Ser16 and

Thr17, the expression of SERCA2, and the phosphorylation of RyR2 at Ser2814. No significant changes were observed in the levels of novex-3, sAnk1, or the expression of RyR2 and its phosphorylation at Ser2808; *t* test, $*p < 0.05$, $**p < 0.01$, $***p < 0.001$; $n = 3$ animals per group; data points represent technical replicas of three different biological samples; GAPDH served as loading control; quantification of phosphorylation levels is presented as absolute phosphorylation levels and normalized to total PLN or RyR2 levels. *Pent* pentamer, *Mono* monomer, *Tot* total